Comparative analysis of transmittance measurement geometries and apparatus

Marjan Shahpaski[1], Luis Ricardo Sapaico[2] and Sabine Süsstrunk[1]
[1]School of Computer and Communication Sciences, EPFL
[2]Océ Print Logic Technologies S.A.
{marjan.shahpaski, sabine.susstrunk}@epfl.ch, ricardo.sapaico@oce.com

Abstract

The accurate measurement of reflectance and transmittance properties of materials is essential in the printing and display industries in order to ensure precise color reproduction. In comparison with reflectance measurement, where the impact of different geometries (0°/45°, d/8°) has been thoroughly investigated, there are few published articles related to transmittance measurement. In this work, we explore different measurement geometries for total transmittance, and show that the transmittance measurements are highly affected by the geometry used, since certain geometries can introduce a measurement bias. We present a flexible custom setup that can simulate these geometries, which we evaluate both qualitatively and quantitatively over a set of samples with varied optical properties. We also compare our measurements against those of widely used commercial solutions, and show that significant differences exist over our test set. However, when the bias is correctly compensated, very low differences are observed. These findings therefore stress the importance of including the measurement geometry when reporting total transmittance.

Introduction

Transmittance measurement is used in a wide range of industries, from solar cells [1] and light filter manufacturing [2] to quality control in food production [3]. The accurate characterization of transmittance is especially important for applications that depend on backlight illumination, which are created by depositing an image onto a substrate that is illuminated from the back side. Common backlit devices include LCD displays [4] and printed advertisements [5]. The correct display on these devices requires accurate spectral prediction models, and transmittance measurements are used extensively in their calibration [6, 7, 8, 9].

Materials generally transmit light in both direct and diffuse manner, and both have to be captured for *total* transmittance measurement. The diffusion is caused by intrinsic light scattering and by rough material interfaces. This causes light to leave the material in all directions of the hemisphere, with varying intensities.

The most common method for capturing *total* transmittance is by using integrating spheres, whose interior is coated with a highly reflective and almost Lambertian material. After numerous bounces inside the sphere, all light that leaves the measured sample is averaged, which is then measured by a spectrometer. Capturing total transmittance requires proper measurement setup and diligence. For that reason, several works and industrial standards have been developed that carefully outline the necessary steps for its capture [10, 11, 12, 13, 14]. All these approaches are based on integrating spheres.

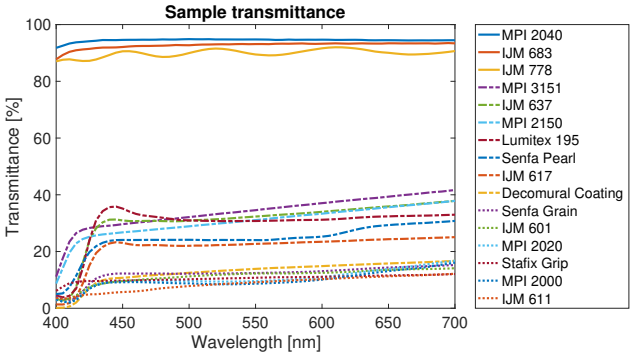

Figure 1: Total transmittance of our diverse set of samples. The samples include smooth transparent plastics, milky plastics, papers and textiles. The measurements were performed with our custom setup in the 0°/d geometry. Best viewed on color display.

In [1], Yu et al. compare the results of the above mentioned industrial standards for haze estimation, which depends on total transmittance measurement. Additionally, they compare their accuracy for measuring total transmittance. Apart from this work, the influence of measurement geometries remains too rarely addressed. We therefore present one of the first comparisons of different geometries for total transmittance measurement.

The main objective of our work is to quantify the impact that differences in measurement geometry have on the measured transmittance values. We are interested in measuring the total transmittance, i.e., both direct and diffuse components, as our goal is to measure the total amount of light that leaves the samples. We have therefore built a custom setup, which is easily modifiable and allows us to gain insights into how much the different effects, existing for different measurement geometries, affect the results. We evaluate their performance over a set of samples with different transmitting properties, whose total transmittances are shown in Figure 1. These samples include smooth transparent plastics, milky plastics, papers, and textiles. We show that the various geometries provide measurements with non-trivial differences.

Our secondary objective is to analyze which configuration yields results that are closest to those of commercial spectrophotometers, which employ various measurement geometries. The comparisons show that there are notable differences even between the commercial solutions. Some measurement geometries introduce a significant measurement bias, which should be compensated. Total transmittance thus depends on the measurement geometry and should to be reported with it.

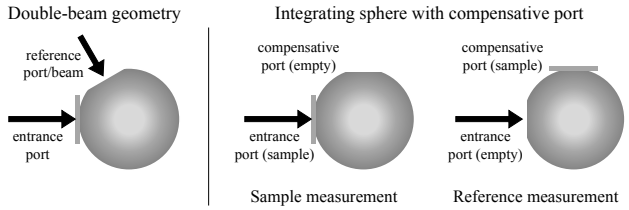

Figure 2: Comparative methods for measuring total transmittance maintain a constant sphere reflectance when taking the reference and sample measurement. Left: Double beam geometry. A second illuminating beam is used to perform the reference measurement. Right: Integrating sphere with compensation port. The sample is switched between the entrance and compensative ports for the sample and reference measurements, respectively.

Measuring total transmittance

In order to define the transmitting properties, different aspects of material transmittance can be measured, such as *direct*, *diffuse*, and *total* transmittances, *haze* and *clarity*. Direct transmittance measures the amount of light that leaves the sample in the same direction as the incident beam direction, i.e., without being scattered. Diffuse transmittance measures the light that is scattered by the sample in all directions except the direct. Total transmittance is the sum of the direct and the diffuse components. Haze describes the wide-angle scattering (at an angle greater than 2.5° from incident beam direction [13]) and is calculated as the ratio of diffuse to total transmittance. Finally, clarity compares the light flux intensity subjected to narrow angle scattering (excluding 0°) to the directly transmitted flux.

Direct transmittance can simply be measured by a collimated light source and a spectrometer. Attempting to measure total transmittance with an apparatus built for direct transmittance will capture only the direct component, and all scattered light will be lost. This will yield much lower transmittance values compared to the true sample transmittance for scattering samples. Therefore, the measurement of total transmittance (along with diffuse transmittance and haze) requires a more complicated apparatus, such as goniometer-based or integrating sphere-based methods.

Instruments capable of measuring total transmittance can employ *comparative* or *substitutive* methods. Within each method, there are different measurement geometries. Two representative geometries for the comparative method are shown in Figure 2. The left side of Figure 2 shows the schema of the double beam geometry. It uses a collimated or converging light beam to illuminate the sample that is placed at the entrance port of the integrating sphere. In addition, while the sample is still placed at the entrance port, there is a second unobstructed entrance through which an equivalent light beam is sent to take the reference measurement. This allows for the measurement of the sample and the reference while maintaining the same average sphere reflectance. Therefore, it produces highly accurate measurements.

Another measurement geometry within the comparative methods is shown on the right side of Figure 2. It uses a single beam in combination with an integrating sphere that features a compensative port. The compensative port is empty while the sample measurement is taken, and it is populated by the sample when the reference measurement is taken, maintaining a constant average sphere reflectance.

The substitutive methods generally require simpler measurement setups, since they use a single beam and integrating spheres without additional ports, apart from the entrance and measurement ports. However, this requires the samples to be removed from the entrance port when taking the reference measurement. Example geometries are featured in Figure 4. This substitution creates a difference in the average sphere reflectance between the two measurements, since the empty port has zero reflectance, while the sample has a non-zero reflectance. More concretely, the light flux that radiates from the sample gets reflected from the sphere wall to irradiate the back side of the sample, which then reflects back some of this light into the sphere. This light flux is read by the sensor and reported as a higher transmittance value. Corrections have been proposed [15], which require the hemispherical reflectance of the measured sample. They can be extended by incorporating the diffuse and direct components of the sample transmittance, and the degree of sphere wall diffusion [16].

Sphere radiance

The difference between these two classes of methods can be shown formally. The radiance L of an internally illuminated sphere has the following expression [17]:

$$L = \frac{\Phi}{\pi A} M, \tag{1}$$

where Φ is the incident radiant flux, A is the sphere surface area and π is the total projected solid angle from the sphere surface, assuming a Lambertian reflectance. If we multiply the fraction from this equation by a surface reflectance, we can compute the radiant flux of a diffusely reflecting surface. However, the radiance of the sphere is increased by a sphere multiplier M, because each sphere spot is reflective and therefore radiating. The sphere multiplier is computed as follows [1]:

$$M = \frac{\rho^o}{1 - \rho^s \left(1 - \sum_{i=0}^{n} f_i\right) - \sum_{i=0}^{n} \rho_i f_i}, \tag{2}$$

where ρ^o is the surface reflectance for the incident light flux, ρ^s is the reflectance of the internal sphere wall, ρ_i is the reflectance of port i, and f_i is the fraction of port i to the total sphere area. If the incident beam illuminates the sphere wall, $\rho^o = \rho^s$. Equation 2 accounts for the increase in radiance due to multiple reflections, and can also be regarded as the average number of bounces of a photon inside the sphere before it is absorbed or it escapes.

From Equation 2 we can see that the reference and sample measurements with the substitution methods are subjected to different average sphere reflectance. When taking the reference measurement, all sphere ports have a zero reflectance, thus the sum featuring ρ_i equals zero. However, when a sample is present at the entrance port, we must include its reflectance as the corresponding ρ_i. This yields a higher sphere multiplier M. In contrast, the comparative methods maintain the same average sphere reflectance for both reference and sample measurement.

Another observation from Equation 1 is that as we decrease the size of the sphere, A, we increase its radiance. However, this comes at a cost, since smaller spheres have a lower sphere multiplier due to their larger port fraction f. This makes it more difficult for smaller spheres to distribute ("integrate") the radiance uniformly across their inner surface, and thus are more dependent on the incident light flux distribution.

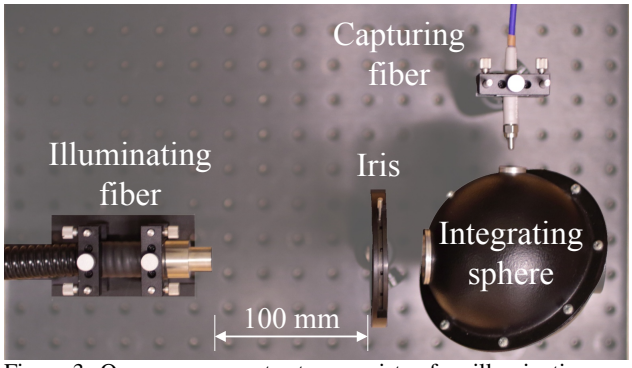

Figure 3: Our measurement setup consists of an illuminating optical fiber, an iris diaphragm or opal glass (configuration dependent), an integrating sphere and a capturing optical fiber connected to a spectrometer. Depicted is the configuration 0°/d.

Our measurement setup

Our approach for measuring the total transmittance follows the ASTM D 1003 standard [13]. We are restricted by the design of our integrating sphere to use a substitutive method. Nevertheless, our study compares the influence of different geometries given the same sphere design. We also compare the results from this modular setup to commercial measurement instruments (Agilent Cary 5000 and X-Rite Color i7).

For our experiments, we built a custom optical setup, whose main components are visualized in Figure 3. It consists of an illuminating optical fiber connected to a Dolan-Jenner DC-950-HR illuminator, an iris diaphragm or opal glass (configuration dependent), an integrating sphere and an optical fiber connected to a Maya2000 Pro spectrometer.

To approximately collimate the incident illumination, we use an iris diaphragm at a distance of 100 mm from the illuminating fiber. This creates a light beam of approximately 8 mm in diameter at the entrance port of the sphere. Due to subsurface scattering, the light can travel an additional 8.5 mm radially across the sample plane before overfilling the entrance port. To create a diffuse illumination instead, we exchange the iris diaphragm by a diffusing opal glass. This configuration illuminates the sample across its entire surface. Note that this results in an approximately diffuse illumination, since the opal glass' size is finite, and thus not all incident angles are present. The diffuse illumination in the third configuration (see Figure 4c) is achieved by both the opal glass and the integrating sphere, and it is therefore uniform. The illumination did not include UV radiation.

The integrating sphere has a diameter of 100 mm and includes one port of 25 mm and one port of 10 mm diameter. Thus, the port fraction of our sphere is $f = 1.84\ \%$. The two ports are located on its equator, separated by 90°. The sphere's inside is coated with a highly reflective and diffusing coating.

The output optical fiber has a 25.4° field-of-view (≈f/5), and is protected from direct incident illumination by a baffle. The sphere does not have baffling against first bounce radiance. Therefore, we keep the fiber slightly outside of the integrating sphere, while keeping its field-of-view completely inside the sphere.

We connect the output fiber to the Maya2000 Pro spectrometer for capturing the data. We used a temporal averaging of 5 captures and we applied a spectral boxcar smoothing filter of 10 samples length. The spectrometer captures UV, visible and NIR

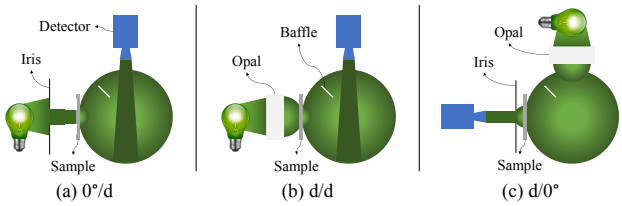

(a) 0°/d (b) d/d (c) d/0°

Figure 4: The set of measurement geometries that we have evaluated with our custom setup. They enable us to capture total transmittance. The details of these geometries can be found in Table 1.

information from 200 nm to 1120 nm, with a step of 0.5 nm, totaling 2068 samples. Since we are interested only in the visible part of the spectrum, we disregard the captured spectra outside of the range 400 nm to 700 nm, and lower the spectral resolution to 5 nm. This allows us to compare to the commercial spectrophotometers.

The three measurement configurations that we evaluated with our modular setup are listed in Table 1. Furthermore, they are graphically illustrated in Figure 4. In the 0°/d geometry (see Figure 4a), we place the sample at the sphere entrance port (25 mm). It is then illuminated with a collimated beam of light. The sphere integrates the complete light flux that leaves the sample, and we read the radiance of the sphere wall with the spectrometer. In the d/d geometry, shown in Figure 4b, we illuminate the sample with a partially diffuse incident light flux, which we create by placing the opal glass in front of the sample. Finally, in the 0°/d geometry (Figure 4c), the sample is illuminated with a completely diffuse light flux, since we place it at the sphere's exit port (25 mm). Note that in 0°/d we switch the entrance and exit ports to maintain equal area of the sample port across geometries.

In addition to studying the effects of different measurement configurations, we also compare our results to those from commercially available solutions, namely the Agilent Cary 5000 and the X-Rite Color i7. The Cary 5000 spectrophotometer uses a double beam and a 0°/d measurement geometry. Our measurements were performed with its internal DRA (Diffuse Reflectance Accessory) that includes an integrating sphere of 110 mm diameter. The captured spectra contain information inside the 400 nm to 700 nm spectral range, with a resolution of 5 nm. Unlike our illumination source, the one in the Cary includes UV radiation.

The Color i7 uses a d/0° geometry. This geometry can also be used for measuring total transmittance due to reciprocal optical geometry, where the hemispherical detector's field-of-view (0°/d) is replaced by a hemispherical input flux (d/0°). This geometry has an advantage of greater incident light flux, since the integrating sphere collects most of the light from the illuminant. The integrating sphere has a diameter of 6 inch (152.4 mm). We again extract the measured information from 400 nm to 700 nm, and adjust the measurements' resolution from 10 nm to 5 nm by interpolation. The UV filter was inserted for all measurements.

Table 1: The measurement configurations (geometries) that we used to capture total transmittance with our setup.

Geometry	Illumination	Capture	Sample position
0°/d	collimated	diffuse	sphere entrance
d/d	diffuse	diffuse	sphere entrance
d/0°	diffuse	direct	sphere exit

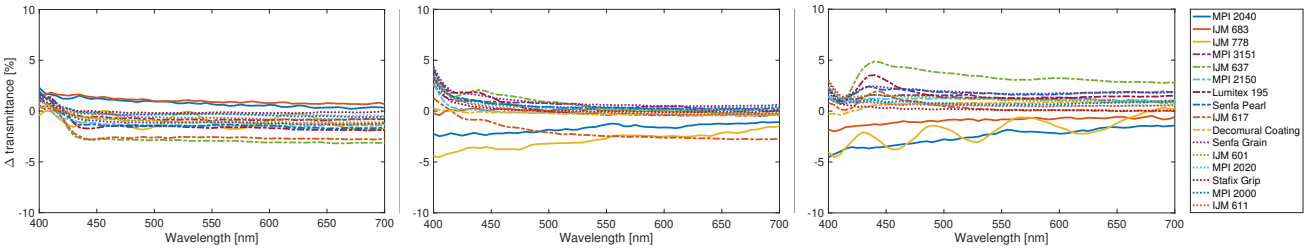

(a) 0°/d vs. d/d : MAE = 1.11 %

(b) 0°/d vs. d/0° : MAE = 0.81 %

(c) d/d vs. d/0° : MAE = 1.31 %

Figure 5: Inter-configuration differences. These figures show the differences in transmittance between the different geometries of our transmittance measurement setup. Positive values translate into higher transmittance measurements for the first measurement geometry. The geometries are presented in Table 1. A numerical breakdown of the accuracy can be found in Table 2. Best viewed on color display.

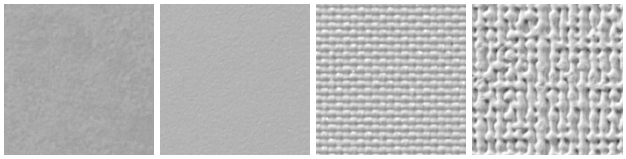

(a) IJM 683 (b) MPI 3151 (c) Lumitex 195 (d) Decomural Coating

Figure 6: An example set of sample surface texture and appearance. Note that the test samples are very varied to allow us to properly evaluate the accuracy of the different measurement geometries and apparatus.

Experiments and results

For our experiments, we created a test set of 16 samples based on their varied reflecting, absorbing and scattering characteristics. The list of samples together with their total transmittance can be found in the legend of Figures 1 and 5, where they are sorted by their average transmittance. The samples are fairly devoid of color, since they are used as print media. In the following, we consider the first three samples to be transparent, and the rest to be diffusing.

An example set of the samples' surface texture can be seen in Figure 6. The IJM 683 is a glossy, transparent, adhesive plastic film. MPI 3151 is a satin, white, translucent, adhesive vinyl. The Lumitex 195 is a fine coated polyester fabric, and the Decomural Coating is a matt, textured vinyl with a very rough surface.

Inter-configuration differences

Table 2 compares the transmittance measurements of the set of samples obtained using our custom setup. The measurement geometries that we used are detailed in Table 1. We compare the differences over all samples, but we also show them for only the transparent and diffuse sets of samples. For computing the differences, we used the MAE, RMSE, and ΔE_{00} error metrics. The transmittance values were expressed in percentage.

A more comprehensive comparison of the measurement differences can be found in Figure 5. It shows the difference for every sample, over the complete spectrum, when measured in the stated configurations. Positive values translate into higher transmittance measurements for the first measurement geometry. For example, in Figure 5a, positive values mean that the 0°/d geometry measured higher transmittance values than the d/d geometry, and the opposite is true for the negative values.

We can see that the difference between the configurations that use diffuse capture is not very significant, although we change the illumination from collimated to diffuse. The differences are slightly more pronounced for the diffuse samples than for the transparent samples. In Figure 5a we can see that there is a bias in the measurements. The d/d geometry consistently measures higher transmittance for the diffusing samples, with a median difference of -0.84 %. In the remainder of the text, we use the term *bias* to refer to the median difference across a set of measured samples. If we remove this bias, i.e., subtract 0.84 % from all d/d measurements, the MAE decreases to 0.85 %. In these two configurations, the average sphere reflectance is consistent between the measurements of the same sample, and the only difference is in the distribution of the incident light flux.

In the second row of Table 2 we notice that the MAE between 0°/d and d/0° is less than 1 %. On a closer inspection, we see that the transparent samples show larger differences than the diffuse samples. Figure 5b shows us that two of the three transparent samples appear to have higher transmittance when measured with d/0°. On the other hand, we note that the spread of errors for the diffuse samples is low, thus the measurements are consistent. The bias across all samples is 0.06 %. If we remove MPI 2040, IJM 778, and IJM 617, we arrive to a MAE of 0.48 %.

The differences between d/d and d/0° are the most pronounced. In Figure 5c, we see both previous effects in this case, i.e., the transmittance of the transparent samples is greater for d/0°, and there is a measurement bias of 0.85 % for d/d. These factors contribute to the greatest MAE of 1.31 %. After correcting for the bias, the MAE decreases to 1.02 %.

All geometries maintain equal average sphere reflectance when measuring the same sample. From this we conclude that the measurement bias is inherent to the d/d geometry. It is likely caused by multiple reflections between the samples and the opal glass. These reflections do not occur in the other two geometries (see Figure 4). Therefore, care must be taken when positioning the elements in the measurement setup.

Table 2: Inter-configuration differences. This table compares the measurements performed with the geometries from Table 1. The results are evaluated over the set of samples shown in Figure 1.

Geometry	All samples			Transparent			Diffuse		
	ΔE_{00}	RMSE	MAE	ΔE_{00}	RMSE	MAE	ΔE_{00}	RMSE	MAE
0°/d vs. d/d	1.05	1.35	1.11	0.32	1.06	0.94	1.22	1.41	1.15
0°/d vs. d/0°	1.24	1.24	0.81	0.49	1.99	1.56	1.41	0.99	0.64
d/d vs. d/0°	1.44	1.61	1.31	0.66	2.06	1.77	1.62	1.48	1.20

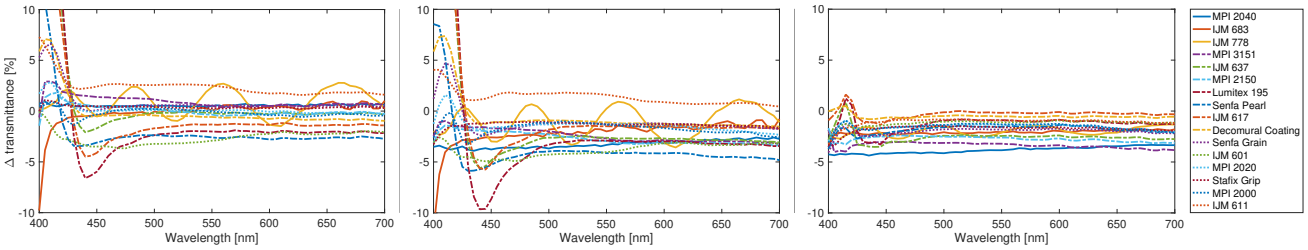

(a) Cary 5000 vs. Color i7 : MAE = 1.48 %

(b) Cary 5000 vs. 0°/d : MAE = 2.62 %

(c) Color i7 vs. 0°/d : MAE = 1.85 %

Figure 7: Inter-spectrometer differences. These figures show the difference in transmittance between the commercial spectrophotometers and our setup in the 0°/d geometry. Positive values translate into higher transmittance measurements for the first measurement apparatus. A numerical breakdown of the accuracy can be found in Table 3. Best viewed on color display.

Inter-spectrometer differences

Table 3 summarizes our comparisons to commercial spectrophotometers. We have selected the 0°/d geometry of our setup for these comparisons, because it showed the best accordance to both the Cary 5000 and the Color i7. Here it is interesting to observe that the commercially available spectrophotometers have a similar measurement difference between their measurements as well as to those from our setup.

In Figure 7a, we can see that there is a negligible bias between the Cary 5000 and the Color i7 measurements, amounting to 0.03 %. An obvious error source can be seen in the shorter wavelengths, between 400 nm and 450 nm. This error stems from the fact that the measurements with the Cary 5000 were performed under illumination that included UV radiation, however, for the Color i7's measurements the UV radiation was filtered out. These differences come from fluorescence, since some of the samples fluoresce. If, for a better comparison, we consider only the wavelengths from 500 nm to 700 nm, then the MAE comes down to 1 %. By removing the bias, we see an insignificant MAE decrease to 0.99 %.

Continuing to Figure 7b, we can see that there is a prominent measurement bias. Since our 0°/d setup uses a substitution measurement method, this bias is caused by the non-constant average reflectance of the integrating sphere between the reference and sample measurement. The light that reflects from the sample's interface back into the sphere increases the measured transmittance, since we measure the radiance of the sphere wall. The bias amounts to -1.95 %, i.e., 1.95 % higher median transmittance for 0°/d. When we remove it from the measurements, the MAE becomes 1.58 %, which is comparable to the Cary 5000 vs. Color i7 difference. In this comparison, we again have the errors in the short wavelengths caused by the UV illumination of the Cary 5000. If we compare the measurements in the 500 nm to 700 nm wavelength range, we obtain a MAE of 2.22 %, or 1.07 % after also removing the bias of the 0°/d measurements.

Table 3: Inter-spectrometer differences. This table compares the measurements performed with two commercial spectrophotometers and our measurement setup in the 0°/d geometry. The results are evaluated over the set of samples shown in Figure 1.

Spectrometer	All samples			Transparent			Diffuse		
	ΔE_{00}	RMSE	MAE	ΔE_{00}	RMSE	MAE	ΔE_{00}	RMSE	MAE
Cary 5000 vs. Color i7	1.76	2.92	1.48	0.38	1.27	0.83	2.07	3.18	1.63
Cary 5000 vs. 0°/d	2.75	3.51	2.62	0.72	2.65	2.30	3.22	3.68	2.69
Color i7 vs. 0°/d	1.82	2.09	1.85	0.67	2.77	2.62	2.08	1.90	1.68

Table 4: Updated inter-spectrometer differences. This table updates the results from Table 3 by considering the various sources of error in order to provide a better comparison between the measurement apparatus. The results are evaluated over all samples. The effects shown in the table header are cumulative.

Spectrometer	Original		500-700nm		Bias	
	RMSE	MAE	RMSE	MAE	RMSE	MAE
Cary 5000 vs. Color i7	2.92	1.48	1.33	1.00	1.31	0.99
Cary 5000 vs. 0°/d	3.51	2.62	2.45	2.22	1.33	1.07
Color i7 vs. 0°/d	2.09	1.85	2.01	1.77	0.96	0.76

Finally, in Figure 7c we compare the measurements from the Color i7 and our 0°/d geometry. We again see the effects already encountered in the previous comparisons. Namely, the 0°/d has a measurement bias of 1.75 %, somewhat lower when compared to that of the Cary 5000. However, we do not see the errors in the short wavelengths, since both measurements were performed in the absence of UV radiation. If we correct for the measurement bias, we achieve a MAE of 0.79 %. For a complete comparison, we also compute the MAE over the 500 nm to 700 nm range, which amounts to 0.76 %.

An updated comparison table that takes into account the previously discussed effects is shown in Table 4. The effects listed in the table header are cumulative. They represent the original results over all 16 test samples, evaluating the differences on the 500 nm to 700 nm wavelength range, and removing the measurement bias. The final column (Bias) incorporates the effects from the previous one. Although the start and end differences are comparable, the effects that exist for the various measurement setups are different. The table outlines the bias that exists in our implementation of the 0°/d geometry, which is based on a substitutive method.

Repeatability

We compared the measurements of the samples done with our 0°/d setup over a span of more than one month, and note that there are negligible differences, comparable to those of the commercial spectrophotometers. We report the differences in Table 5. The MAE between our measurements in the 0°/d configuration performed on 29.03.2018 and 09.05.2018 is 0.33 %. The MAE between the measurements of the same set of samples done with the Color i7 spectrophotometer done on 29.11.2017 and 14.03.2018 is also 0.33 %.

Table 5: Measurement repeatability. We report the average difference over the same set of measured samples that were taken with a time difference of at least one month.

Spectrometer	ΔE_{00}	RMSE	MAE
0°/d	0.58	0.48	0.33
Color i7	0.37	0.39	0.33

Conclusion

In this work, we discussed the effects that influence the accuracy of total transmittance measurements for various measurement methods and geometries that use integrating spheres. To show the differences in practice, we constructed a custom optical setup that can be configured to the 0°/d, d/d, and d/0° geometries. These were based on a single beam substitutive measurement method. We evaluated their accuracy over a test set of 16 samples that have various levels of transmittance, absorbance and reflectance. The measurements showed a MAE as low as 0.81 % between 0°/d and d/0°, and up to 1.31 % between the d/d and d/0° geometries. We noted that the d/d geometry consistently measured higher transmittances than 0°/d and d/0°, whose measurements did not show an apparent bias. This is likely caused by our implementation of the geometry, which introduced multiple reflections between the sample and the opal glass. Therefore, care must be exercised when building custom measurement setups.

We also compared the results obtained by our setup to those of commercial spectrophotometers, the Agilent Cary 5000 and the X-Rite Color i7. The 0°/d geometry had the best measurement accordance to the commercial solutions, which is also the geometry that the Cary 5000 uses. However, the Cary has a double-beam configuration (comparative method), and our setup has a single beam configuration (substitutive method). At first glance, all spectrometers showed similar differences in their measurements. However, those inconsistencies were caused by different effects. Our 0°/d geometry showed a measurement bias because of varying average reflectance of the integrating sphere during reference and sample measurements. This is caused by the nature of the substitution methods, and in our experiments lead to a MAE of up to 2.22 %. After correcting for these effects, all apparatus performed to a MAE of 1.07 % or less.

When reporting total transmittance it is thus good practice to also include the measurement geometry. As we have shown, some measurement geometries introduce a significant bias. However, if it is compensated, very low errors can be achieved.

Acknowledgments

We would like to thank Théo Phan Van Song from Océ Print Logic Technologies SA for providing us with the Cary 5000 measurements of our samples.

References

[1] H. L. Yu and C. C. Hsaio. Comparison of different measurement methods for transmittance haze. Metrologia, 46, 4 (2009).

[2] J. C. Travis, N. K. Winchester and M. V. Smith. Determination of the transmittance uniformity of optical filter standard reference materials. Journal of research of the National Institute of Standards and Technology, 100, 3 (1995).

[3] J. P. Wold, T. Jakobsen and L. Krane. Atlantic salmon average fat content estimated by near-infrared transmittance spectroscopy. Journal of Food Science, 61, 1 (1996).

[4] H. Kawamoto. The history of liquid-crystal displays. Proceedings of the IEEE, 90, 4 (2002).

[5] W. Dunn. Advertising displays. U.S. Patent No. 8,016,452 (13 Sep. 2011).

[6] M. Hébert and R. D. Hersch. Yule-Nielsen based recto–verso color halftone transmittance prediction model. Applied optics, 50, 4 (2011).

[7] J. Machizaud and M. Hébert. Spectral reflectance and transmittance prediction model for stacked transparency and paper both printed with halftone colors. JOSA, 29, 8 (2012).

[8] M. Hébert and J. Machizaud. Spectral reflectance and transmittance of stacks of nonscattering films printed with halftone colors. JOSA, 29, 11 (2012).

[9] S. Mazauric, M. Hébert, L. Simonot and T. Fournel. Two-flux transfer matrix model for predicting the reflectance and transmittance of duplex halftone prints. JOSA, 31, 12 (2014).

[10] L. Hanssen. Integrating-sphere system and method for absolute measurement of transmittance, reflectance, and absorptance of specular samples. Applied Optics, 40, 19 (2001).

[11] International Organization for Standardization. Plastics - Determination of Haze of Transparent Materials. ISO 14782 (1997).

[12] Japanese Industrial Standard. Plastics - Determination of the Total Luminous Transmittance of Transparent Materials - Part 1: Single Beam Instrument, JIS K 7361-1 (1997).

[13] B. Geometries and S. Abrasion. Standard test method for haze and luminous transmittance of transparent plastics. ASTM Int 1 (2012).

[14] H. L. Yu, C. C. Hsaio and W. C. Liu. New apparatus for haze measurement for transparent media. Measurement Science and Technology (2006).

[15] J. G. Symons, E. A. Christie and M. K. Peck. Integrating sphere for solar transmittance measurement of planar and nonplanar samples. Applied optics, 21, 15 (1982).

[16] K. Grandin and A. Roos. Evaluation of correction factors for transmittance measurements in single-beam integrating spheres. Applied optics, 33, 25 (1994).

[17] A. V. Arecchi, T. Messadi and R. J. Koshel. Field Guide to Illumination. SPIE Press, Bellingham, WA, 2007.

Author Biography

Marjan Shahpaski is a PhD student at the École Polytechnique Fédérale de Lausanne (EPFL, Switzerland). His research activity is focused on 3D reconstruction with structured-light and the measurement and estimation of BTDF.

Luis Ricardo Sapaico obtained his Ph.D (Computer Science) from the Tokyo Institute of Technology in 2011. He currently works as an Imaging Scientist at Océ Print Logic Technologies in Créteil, France. His main research interests are in color science, computer vision and image processing.

Sabine Süsstrunk is a full professor and Director of the Images and Visual Representation Laboratory (IVRL) in the School of Computer and Communication Sciences at EPFL. Her main research areas are in computational imaging, computational photography, color image processing and computer vision, multimedia, and computational image quality and aesthetics. She is a Fellow of IEEE and IS&T.